Mem. S.A.It. Vol. 80, 59

Memorie della

Near-infrared, IFU spectroscopy of the molecular gas in HH99B

T. Giannini, L. Calzoletti, and B. Nisini

Istituto Nazionale di Astrofisica – Osservatorio Astronomico di Roma, Via Frascati 33. I-00040 Monte Porzio Catone, Italy, e-mail: giannini@oa-roma.inaf.it

Abstract. We have characterized the morphology and the physical parameters governing the shock physics of the Herbig-Haro object HH99B through SINFONI-SPIFFI IFU spectroscopy ($R \sim 2000 - 4000$) between 1.10 and 2.45 μm. More than 170 emission lines have been detected, that, to a large extent, have never observed before in a Herbig-Haro object. Most of them come from ro-vibrational transitions of molecular hydrogen ($v_{up} \leq 7$, $E_{up} \leq 38\,000$ K). In addition, we observed several hydrogen and helium recombination lines, along with fine-structure lines of ionic species. Here we present the results obtained from the analysis of the H_2 lines. These were interpreted in the framework of Boltzmann diagrams, from which we have derived extinction and temperature maps. We find that at the bow apex thermalization has been reached at T$\sim$ 6000 K, likely due to the presence of a fast non-dissociative shock. In contrast, different temperature components are simultaneously along the flanks. A decrease in about a factor of ten is registered in the H_2 column density going from the shock wings toward the apex. Both these circumstances are not accounted for by models that have attempted at interpret the H_2 emission in HH99B on the basis of fewer lines. Therefore, the conclusions of these models should be tested in the light of this new piece of information. Finally, from the line intensity map of a bright H_2 line (i.e. 1-0S(1) at 2.122μm) the kinematical properties of the shock at work in the region have been delineated.

Key words. Stars: circumstellar matter – ISM: Herbig-Haro objects – ISM: individual objects: HH99 – ISM: jets and outflows

1. Introduction

Mass loss phenomena in the form of powerful bipolar jets and molecular outflows are often associated with the early evolution of protostars. Along with indirectly regulating the accretion process, they play a crucial role in the interaction between the protostar and the natal environment, causing injection of momentum, kinetic energy, and turbulence in the ISM, as well as irreversible modifications of its chemical structure and physical conditions. The most violent interaction occurs at the terminal working surface (HH object), that often has a curve-shaped morphology (bow-shock). Here the supersonic flow impacts the undisturbed medium and most ambient material is entrained by the jet (e.g. Reipurth & Bally 2001). The large number of parameters that regulate the shock physics (e.g. strength and direction of the local magnetic field, ionization fraction, and den-

Send offprint requests to: T. Giannini

sity gradient between the shocked gas and the local environment) can only be constrained through dedicated observations aimed at probing the physical and kinematical properties of the gas along the whole bow structure. In this respect the Integral Field Spectroscopy (IFU) represents a well-tailored tool, since it allows us to obtain 2-D maps simultaneously at different wavelengths. Here we present the spectral images obtained with the IFU facility SINFONI (Eisenhauer et al. 2003) of a prototype bow-shock, namely the Herbig-Haro object HH99B (Davis et al. 1999, hereafter D99), located in the RCrA molecular core at d∼ 130 pc (Marraco & Rydgren 1981).

2. Observations and results

HH99B was observed with the SINFONI-SPIFFI instrument at the ESO-VLT (Chile) to obtain spectroscopic data in J, H and K bands ($R \sim 2000$, 3000, and 4000, respectively). As a result, we obtained a 3D data-cube containing the HH99B image in more than 170 lines, the large majority being H_2 ro-vibrational lines (121). The detected ro-vibrational transitions come from levels with $v \leq 7$ and E_{up} up to ∼ 38 000 K, many of them never before observed in HH objects. In particular, as we show in Fig. 1 (upper panel), emission of lines with $E_{up} \lesssim 30\,000$ K is present only along the bow flanks, while lines with $E_{up} \gtrsim 30\,000$ K are observed in the whole shock, peaking at the bow head. Therefore, two main results emerge: *(i)* molecular hydrogen also survives where ionic emission is strong (see below), and *(ii)* temperature gradients do exist along the shock, with the highest values reached at the bow head, where stronger excitation conditions are expected to occur. Some examples of atomic lines are depicted in the middle and bottom panels of Fig. 1. Plenty of [Fe II] lines are detected (34 lines), emitted from levels with $E_{up} \lesssim 30\,000$ K. As for H_2, two groups of lines are identified: those with $E_{up} \lesssim 13\,000$ K, which come for the a^4D level, are observed in the whole region, while those at higher excitation energy are only emitted at the bow head. In this same area, emission of hydrogen and helium recombination lines (8 and 3 lines, respectively) along

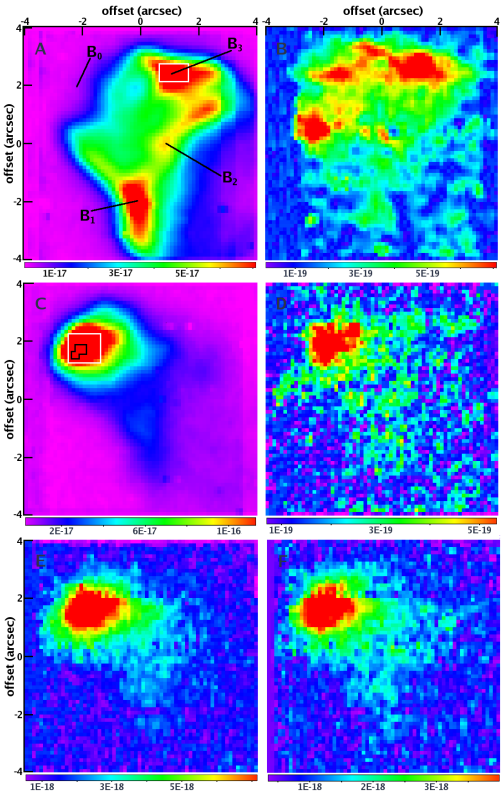

Fig. 1. Selected spectral images from our HH99B data-cube. Intensities are given on a color scale. Offsets are from $\alpha_{2000}=19^h02^m05.4^s$, $\delta_{2000}=-36°54'39''$. A) H_2:1-0 S(1) at 2.122μm. The locations of the knots labeled by D99 are indicated; B) H_2: 2-1S(17) at 1.758μm; C) [Fe II]: $a^4D_{7/2}$-$a^4F_{9/2}$ at 1.644μm; D) [Fe II]: $a^4P_{3/2}$-$a^4D_{7/2}$ at 1.749μm; E) H:Paβ at 1.282μm; F) [P II]: $^2D_2$-$^3P_2$ at 1.188μm.

with fine-structure lines of [P II],[Co II], and [Ti II] are detected.

3. H_2 analysis

3.1. Extinction map

In order to construct *intrinsic* line ratios, we have firstly derived a map of the visual extinction in HH99B. This can be done by using pairs of transitions coming from the same upper level, whose ratio is insensitive to the local physical parameters, depending only on the differential extinction and on the atomic

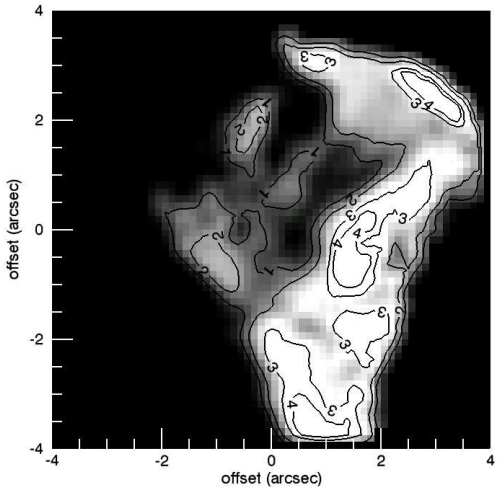

Fig. 2. Extinction map as derived from H_2 line ratios. Contours from A_V=1 to 4 mag are shown.

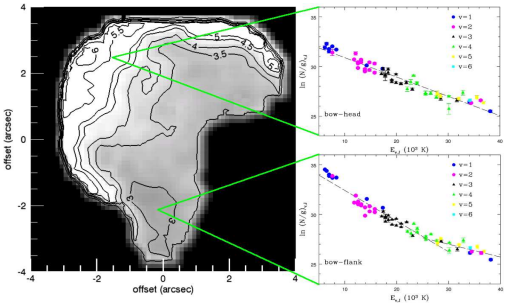

Fig. 3. Temperature map (in 10^3 K) as derived from H_2 line ratios. As an example, we show the rotational diagrams at two points of the bow: while at the bow head H_2 appears thermalized at (T$\sim$ 5000 K), two temperature components co-exist in the southern flank, with an average temperature of $\sim$ 2800 K.

parameters (e.g. Gredel et al. 1994, hereafter G94). The extinction map, obtained by using three line ratios of H_2 bright lines, is shown in Fig. 2, where variations in A_V from 1 to 4 mag can be recognized.

3.1.1. Temperature map

The temperature of the molecular gas can be obtained from a Boltzmann diagram (e.g. G94), plotting $\ln(N_{v,J}/g_J)$ against $E_{v,J}/k$. Here $N_{v,J}$ (cm^{-2}) is the column density of the level (v, J), $E_{v,J}$ (K) its excitation energy and g_J the statistical weight. If the gas is thermalized at a single temperature, the data points align onto a straight line, whose slope gives the gas temperature. We applied this method to all the pixels of the H_2 images, and the resulting map is shown in Fig. 3. Three results can be taken from this map: *(i)* A temperature gradient from $\simeq$ 2 000 K up to 6 000 K occurs from the receding parts of the shock towards the head. We underline that this gradient can be traced because of the very large number of H_2 lines detected, which cover the Boltzmann diagram up to excitation energies of $\sim$ 38 000 K, therefore sensitively widening the dynamical range of temperatures typically probed with H_2 near-infrared lines;
(ii) Two different behaviors in the Boltzmann diagram occur between the bow head and the flanks (see the insets in Fig. 3): H_2 appears fully thermalize (at T$\sim$ 5000 K) at the bow head (hence the contours here give the gas temperature directly), while a curvature exists among the points in the southern flank diagram, so that at least two temperature components can be traced. The outlined behavior can be generalized to the whole bow structure and likely reflects, from one side, that fluorescence can be discarded as a possible excitation mechanism, since it implies strong departures from thermalization (Black & van Dishoeck 1997), and, from the other side, that different shock mechanisms are at work. In fact, the response of the level populations to the shock parameters can be seen in the Boltzmann diagram. Roughly speaking, an enhancement of the shock velocity increases the rate of collisions that vibrationally excite the H_2 molecules and favors thermodynamical equilibrium; thus, the thermalization observed along the head would testify to the presence of a fast shock. The alternative possibility that the observed H_2 emission arises from re-forming H_2 onto dust grains can be reasonably discarded. In fact, the timescale of this process is of the order of 10^{17}/n s^{-1} (Hollenbach & McKee 1979), with n the density of the gas after the compression due to the shock passage. For reasonable values of this parameter (10^4-10^7 cm^{-3}), and assuming a velocity of the downstream gas of the

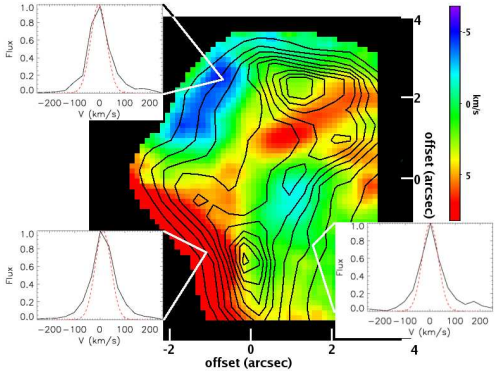

Fig. 4. Local standard of rest (LSR) velocity map of the 2.122μm line peak, with superimposed line intensity contours. Insets show the line profile observed at the bow head (top left), in the southern flank (bottom left), and at the bow center (bottom right). The instrumental profile, measured on OH atmospheric lines, is shown for comparison (red dashed line).

order of 10 km s^{-1}, the distance covered by the gas at the bow head should be between 10^{16} and 10^{19} cm, definitively longer than the linear dimension of knot B0, i.e. $\sim 5\ 10^{15}$ cm.
(iii) A marked difference in the column density of the warm H_2 (from the intercept of the straight line) emerges from the same Boltmann diagrams. For example, from the insets of Fig. 3 we derive $N(H_2) = 2\ 10^{17}$ cm^{-2} and $3\ 10^{16}$ cm^{-2} at the flank and at the bow head, respectively. If the same shock lengths are assumed for these regions, then about 85% of the molecular gas must get destroyed in the most excited part of the shock (although H_2 emission is still observed).

3.2. Kinematical properties

In this section we intend to characterize the kinematical parameters of the shock(s) in HH99B.

Nominally, the spectral resolution of our K band observations would not permit us to resolve the line profile. This limitation, however, is partially compensated by the very high S/N ratio at which we detect the 2.122μm line. A trend in both the peak velocity and in the profile shape can be followed along the bow structure, although we cannot give precise numerical estimates for the line parameters (v_{peak}, FWHM). Our results are presented in Fig. 4, where the contours of the 2.122μm line intensity (de-reddened) have been superposed on the v_{peak} map. Overall the line profile presents a blue-shifted component towards the shock front at the bow head (B0). The opposite occurs along the two flanks and especially along the edge of the B1 flank, where the line peak is shifted $\sim +15$ km s^{-1} with respect to the line profile at the head. The 2.122μm profile does not show double-peaked components, as generally expected for a parabolic bow structure (Schultz et al. 2005), though it does become wider near the center of the bow, where the opposite sides are seen in projection. Here the observed $FHWM_{obs}$ is 85-105 km s^{-1}, that, deconvolved with the instrumental profile, measured on atmospheric OH lines, roughly gives an intrinsic line width of $\sim$ 20-40 km s^{-1}. Along the bow flanks, where the profile width becomes narrower, decreasing toward the spectral resolution limit on the intrinsic width of $\sim$ 20 km s^{-1}. As for the line peak, a sudden increase in $FHWM_{obs}$ is registered at the edge of the southern flank, where we measure up to $\sim$ 115 km s^{-1}, i.e. an intrinsic width of $\sim$ 70 km s^{-1}. This is close to the maximum shock velocity ($\sim$ 80 km s^{-1}) at which H_2 can survive against dissociation (Le Bourlot et al. 2002).

References

Black, J.H., & van Dishoeck, E.F., 1997, ApJ, 322, 412
Davis, C.J., et al., 1999, MNRAS, 308, 539 (D99)
Eisenhauer, F., et al., 2003, SPIE 4841, 1548
Gredel, G., 1994, A&A, 292, 580 (G94)
Hollenbach, D., & McKee, C., 1979, ApJ, 41, 555
Le Bourlot, J., et al., 2002, A&A, 390, 369
Marraco, H.G., & Rydgren A.E., 1981, AJ, 86, 62
Reipurth, B., & Bally, J., 2001, ARA&A, 39, 40
Schultz, A.S., et al., 2005, MNRAS, 358, 1195